CHAPTER 15

Electromechanical Analysis Using Systems Models

While the finite-element techniques of the preceding chapter accurately predict electromechanical behavior of magnetic devices, many engineers need *systems models* instead. Magnetic actuators and sensors are often components in large electromechanical systems such as automobiles, airplanes, power systems, and computers. Design of such systems is carried out nowadays using systems software such as SPICE, MATLAB®, and Simplorer®. Hence this chapter discusses how magnetic actuators and sensors can be modeled with such systems software.

15.1 ELECTRIC CIRCUIT MODELS OF MAGNETIC DEVICES

15.1.1 Electric Circuit Software Including SPICE

Since most magnetic devices are connected to electric circuits, electric circuit simulation software is appropriate. If an equivalent electric circuit can be found for the magnetic device, then it can be inserted in the circuit software. Popular software for modeling electric and electronic circuits includes SPICE, Simplorer, and Multisim. Electric circuits can be used via analogies to also model the magnetic circuits of Chapter 3, heat transfer of Chapter 12, and mechanical motion as described below.

SPICE stands for Simulation Program with Integrated Circuit Emphasis. It is one of the most commonly used electric and electronic circuit simulators. SPICE was originally developed in the early 1970s [1] at the University of California, Berkeley, which has published several SPICE versions in the public domain. Commercial versions include PSPICE, HSPICE, and Maxwell SPICE. At the present time a version of SPICE called TINA-TI™ is available at www.ti.com, and another free version called LT spice is available at www.linear.com. SPICE models have been developed over the years for many electronic circuits and magnetic devices.

Magnetic Actuators and Sensors, Second Edition. John R. Brauer.

15.1.2 Simple *LR* Circuits

As discussed in earlier chapters such as Chapter 9, magnetic devices have an equivalent electric circuit that contains at least one inductance *L.* Any coil has a resistance *R,* usually placed in series with *L.* However, the inductance may be nonlinear, and thus represented as flux linkage versus current. In addition, as the armature moves, the inductance and flux linkage may vary significantly with position.

Example 15.1 SPICE *LR* Model of Axisymmetric Clapper Actuator The DC axisymmetric clapper armature actuator of Figure E7.2.1 is to be modeled in a very simple fashion as an *LR* circuit at the modeled airgap of 2 mm. The coil resistance is 10 Ω. Eddy current losses are to be ignored. The number of turns is 2000. Prepare a SPICE circuit model and use it to find the current as a function of time for 1 s after a 12 V step is applied.

Solution The total energy stored W in Example 7.2 is 0.8604 J for 2000 ampere-turns. Since the number of turns is 2000, the current $I = 1$ A. The inductance is then:

$$L = 2W/I^2 = 1.7208 \text{ H} \tag{E15.1.1}$$

The SPICE circuit model consists of the 1.7208-H inductor in series with the 10-Ω coil resistance, along with a 12-V source turned on at time zero. The circuit developed in Maxwell SPICE is shown in Figure E15.1.1. The computed current versus time is shown in Figure E15.1.2, and shows the expected exponential rise with time constant $L/R = 0.17208$ s.

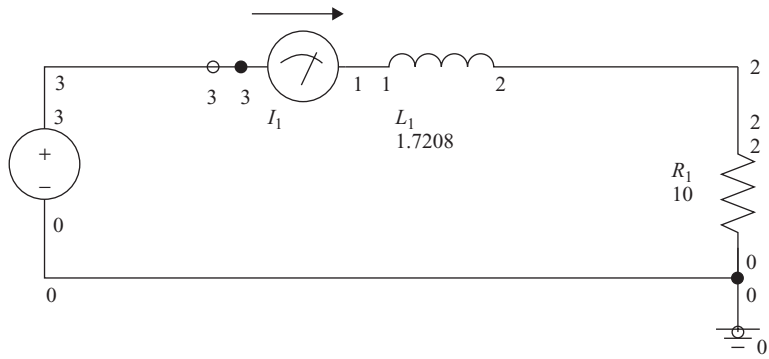

FIGURE E15.1.1 SPICE circuit series *LR* circuit for Example 7.2 at given position.

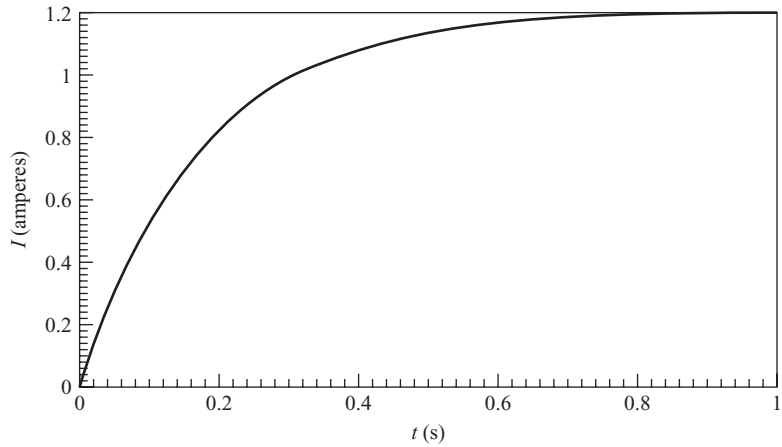

FIGURE E15.1.2 Current waveform computed by SPICE model of Figure E15.1.1.

Example 15.2 Including a Speed Voltage in Example 15.1 The above *LR* circuit is to be modified by including a speed voltage (of polarity to oppose the current) for $t = 0$ to $t = 0.8$ s:

$$V_{\text{speed}} = 10t^2 \tag{E15.2.1}$$

After $t = 0.8$ s the armature stops moving, and thus the above voltage becomes zero. The inductance is assumed to be unchanged from Example 15.1 even though the armature position is changing.

Solution A voltage source is added to the SPICE circuit of Example 15.1, obtaining the circuit shown in Figure E15.2.1. The new voltage source varies with time according to (E15.2.1) and has polarity opposing the original applied voltage. The

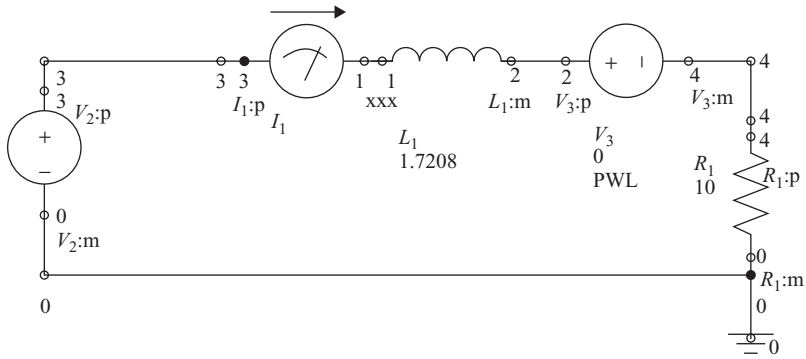

FIGURE E15.2.1 SPICE circuit series *LR* circuit of Example 15.1 with added speed voltage.

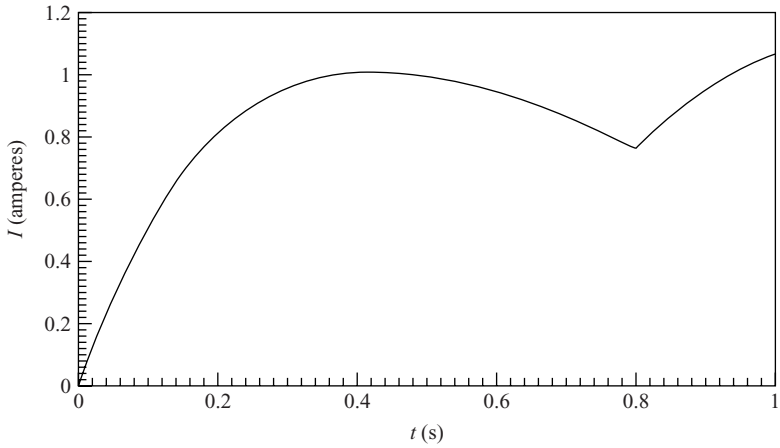

FIGURE E15.2.2 Current waveform computed by SPICE model of Figure E15.2.1.

computed current waveform is shown in Figure E15.2.2. Note that the speed voltage has produced a dip in the current at closure ($t = 0.8$ s), agreeing with the preceding chapter.

15.1.3 Tables of Nonlinear Flux Linkage and Force

In many magnetic actuators and sensors, armature motion causes large changes in flux linkage and inductance. Besides varying with armature position, flux linkage and magnetic force often vary nonlinearly with current because of nonlinear *B–H* curves. Thus current and position are typically two independent parameters which produce variations in flux linkage and force.

To account for such parametric variations, parametric finite-element analysis can be performed. A table of perhaps 20 to 100 different rows, each with a different current or position, can be prepared. Magnetostatic finite-element solutions for flux linkage and force can then be obtained for all table rows. Then for any values of current and position within the table range, interpolation can be done to find the related flux linkage and force.

The electrical performance of the magnetic device is directly affected by flux linkage λ according to Faraday's law. Using the standard voltage sign convention for inductors:

$$V = d\lambda/dt \tag{15.1}$$

Substituting the definition (6.11) for inductance L gives:

$$V = \frac{d}{dt}(LI) = L\frac{dI}{dt} + I\frac{dL}{dt} \tag{15.2}$$

The first term can be considered to correspond with Example 15.1, and the second term is the speed voltage included in Example 15.2. Thus the time variation of flux linkage determines the voltage and/or current waveforms versus time.

15.1.4 Analogies for Rigid Armature Motion

The speed and other mechanical performance parameters of the magnetic device are directly affected by the magnetic forces in the parametric table. However, as discussed in Chapter 12, mass and other mechanical parameters also affect the mechanical performance.

The same electric circuit software used to model the electromagnetic behavior of magnetic devices can also be used by analogy to model the mechanical behavior of rigid armatures. Several analogies are possible. One analogy is based on the structural equation (14.13) simplified for a rigid body with one degree of translational freedom x:

$$M_S \frac{d^2x}{dt^2} + B_S \frac{dx}{dt} + K_S x = F_S \tag{15.3}$$

The analogous equation is for an *RLC* circuit of (14.12) with an additional time derivative taken on both sides:

$$C \frac{d^2V}{dt^2} + \frac{1}{R} \frac{dV}{dt} + \frac{1}{L} V = \frac{dI}{dt} \tag{15.4}$$

Comparing the two analogous equations, the analogy for mass M_S is capacitance C, etc [2]. Thus SPICE and other electric circuit programs can be used to model rigid body motion of armatures of magnetic actuators and sensors [2]. Since the armature, stator, and other parts are all assumed to be rigid bodies, their deformations, strains, and stresses are all assumed to be zero.

15.1.5 Maxwell SPICE Model of Bessho Actuator

The Bessho actuator of Chapter 14 and previous chapters is modeled in Maxwell SPICE as shown in Figure 15.1. The SPICE model was made by exporting parametric tables of flux linkage and force from Maxwell magnetostatic finite-element analyses, represented by the small center icon of the Bessho actuator. The icon produces a speed voltage and a magnetic force. A graph of force versus position for various currents, called pull curves in Chapter 7, is shown in Figure 15.2. Maxwell SPICE automatically interpolates to obtain the force for any airgaps from 0 to 12 mm and for any currents from 0 to 1.21 A.

To the left of the Bessho icon is the electric drive circuit, in this case a 0.5-A current source rising with time constant 20 ms as discussed in previous chapters. To

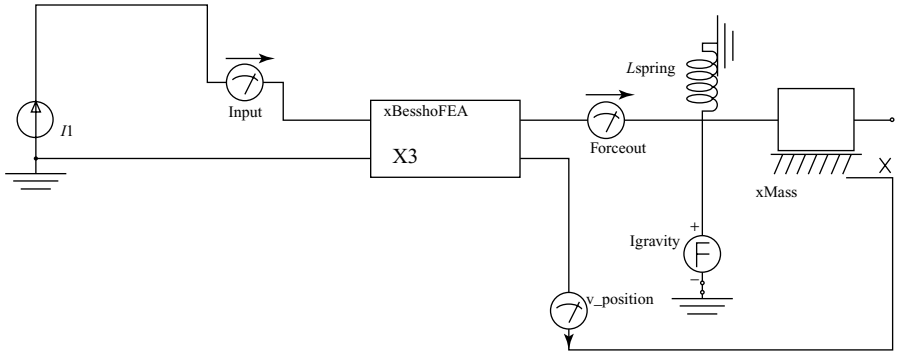

FIGURE 15.1 SPICE model of Bessho actuator. The electrical drive circuit is at the left. The actuator icon represents nonlinear magnetic flux linkage and force tables. The mechanical circuit is at the right.

the right of the Bessho icon is the SPICE analog of the mechanical system, including a mass and optional spring [3].

The circuit of Figure 15.1 does not include any eddy current effects in the conducting steel. Thus its results should be comparable to those of Table 14.1 with zero conductivity. The results of Figure 15.1 computed by SPICE are shown in Figure 15.3. There are four curves, numbered to correspond with cases 1–4 of Table 14.1. The computed closing times of Figure 15.3 differ somewhat from Table 14.1. They agree most closely with the Table 14.1 results for zero conductivity, as they should. The closing times of Figure 15.3 are reduced by 10–15% from those of Table 14.1, possibly due to different meshes and force computation methods. Also, the SPICE model

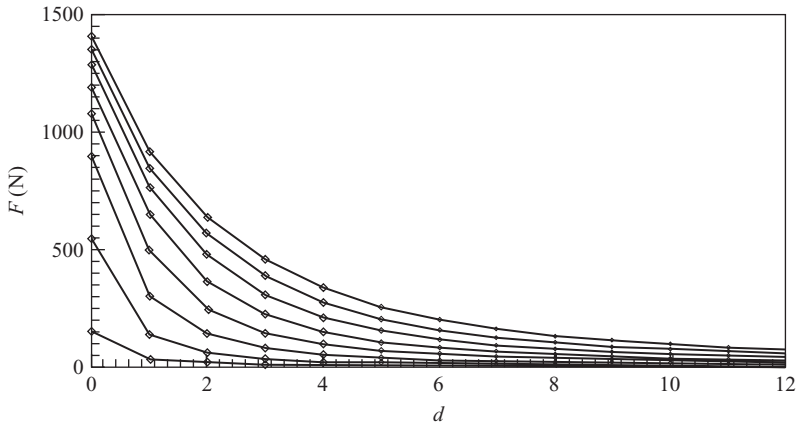

FIGURE 15.2 Pull curves computed by Maxwell parametric finite-element analysis for airgap d ranging from 0 to 12 mm and current I ranging from 0 (the bottom zero pull curve along the horizontal axis) to 1.212 A (the top pull curve).

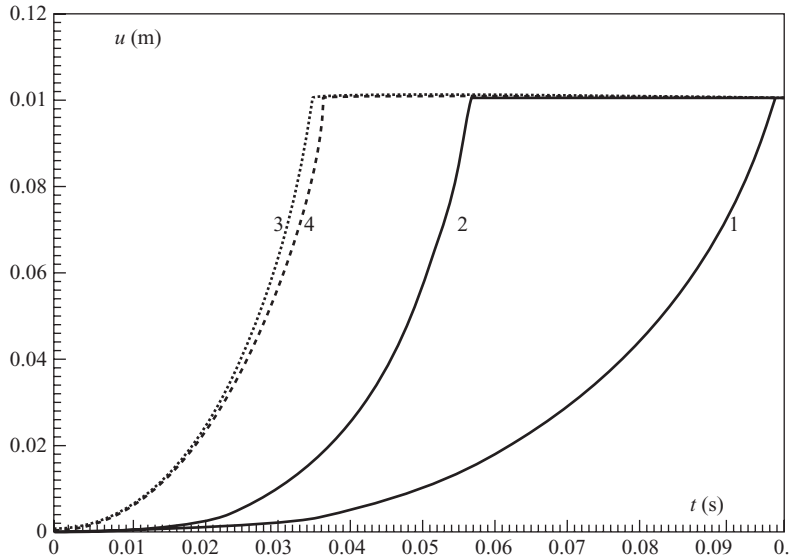

FIGURE 15.3 Computed SPICE results for Bessho armature position versus time. The four cases are those of Table 14.1 with zero conductivity.

of Figure 15.1 does not include any damping B_S or other frictional forces, whereas friction can perceptibly slow down actuator motion.

15.1.6 Simplorer Model of Bessho Actuator

Simplorer is a software package used to design and analyze complex technical systems. Its models can include electric circuit models, models of other physical domains, block diagrams, and state machine structures. One of its languages is the Simplorer Modeling Language (SML). SML is often used to model electromechanical systems, and is here used for the Bessho actuator. Simplorer is a much newer program than SPICE, and its time-stepping algorithms are more likely to converge properly. Also, Simplorer includes a large number of model libraries, including a sensor library. Simplorer instructional material with detailed worked examples is available at www.ansys.com.

The Simplorer SML model of the Bessho actuator is shown in Figure 15.4. Similar to the Maxwell SPICE model of Figure 15.1, it includes an icon of the actuator that represents the Maxwell finite-element model and its flux linkages and forces. To the left of the icon is the electric drive circuit, and to the right is the Simplorer mechanical model.

The Simplorer model was used to predict performance with the 6 kg mass and the 0.5 A input current with 20 ms rise time. The graphs in Figure 15.5 show that the closure time is 97 ms, almost identical to the SPICE results.

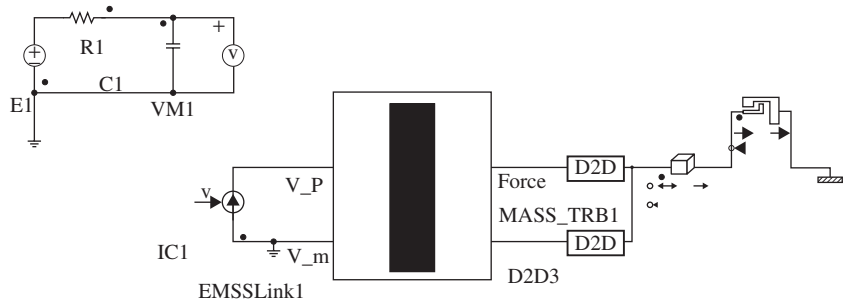

FIGURE 15.4 Simplorer model of Bessho actuator.

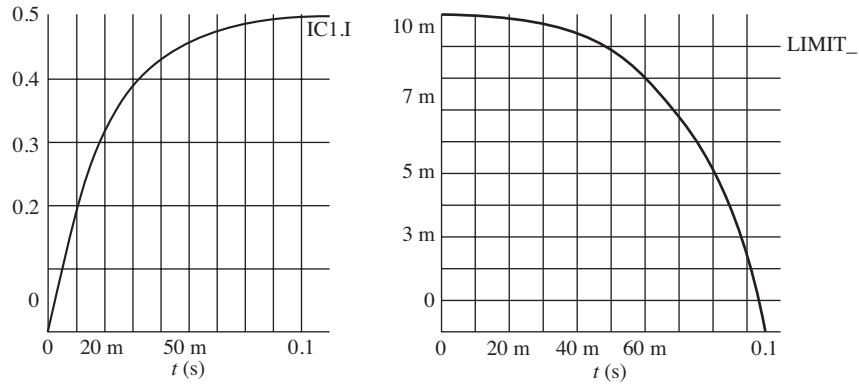

FIGURE 15.5 Computed Simplorer input and output for Bessho actuator with 6-kg moving mass. The input on the left is the current (in amperes) waveform, and the output on the right is the airgap (in meters) as a function of time (in seconds).

15.2 VHDL–AMS/SIMPLORER MODELS

15.2.1 VHDL–AMS Standard IEEE Language

VHDL–AMS stands for Very high speed integrated circuit Hardware Description Language—Analog Mixed Signal. It is a standard language used for describing digital, analog, and mixed-signal systems. It is especially popular for automotive electronic system design.

The IEEE standardized the VHDL-1076 language as a Hardware Description Language for digital models. The VHDL standard from 1993 was extended in 1999 for the description of analog and mixed-signal models in the form of the IEEE 1076.1 standard for VHDL–AMS.

A VHDL–AMS model consists of five basic elements: *entity, architecture, package, package body,* and *configuration*. Multidomain systems, such as the electrical

and mechanical domains of magnetic actuators and sensors, are specified with the appropriate package entries.

The development and simulation of VHDL–AMS models is supported by Simplorer. It contains wizards, importers, exporters, schematics, netlists, digital stimuli, and other VHDL–AMS modeling capabilities. The Simplorer graphical interface contains common basic VHDL–AMS circuit components and blocks. The Simplorer VHDL–AMS solver contains an analog solver, a digital solver, and a controller that controls their interaction [4].

15.2.2 Model of Solenoid Actuator

The standard VHDL–AMS solenoid model is based upon the assumed inductance versus position relation [5]:

$$L(x) = \frac{N^2 L_o}{1 + kx} \tag{15.5}$$

where L_o is the inductance for one turn when airgap $x = 0$, N is number of turns, and k is a dimensionless coefficient. The voltage across the above inductance is:

$$V = \frac{d\lambda}{dt} = \frac{d}{dt}(LI) = N^2 L_o \frac{d}{dt}\left(\frac{I}{1 + kx}\right) \tag{15.6}$$

Since both x and I may vary with time, the above derivative gives:

$$V = N^2 L_o \left[\frac{I}{1 + kx}\frac{dI}{dt} - \frac{Ik}{(1 + kx)^2}\frac{dx}{dt}\right] \tag{15.7}$$

where the second term is the speed voltage.

The magnetic force is given by (5.13), (6.9), and (6.10) as:

$$F = \frac{\partial W_{\text{co}}}{\partial x}, \text{ where coenergy } W_{\text{co}} = \int \lambda dI \tag{15.8}$$

Since the inductance *L(x)* of (15.5) is independent of current, the flux linkage $\lambda = LI$ becomes:

$$\lambda(I, x) = \frac{N^2 L_o I}{1 + kx} \tag{15.9}$$

and the force of (15.8) becomes:

$$F = \frac{N^2 L_o I^2}{2} \frac{\partial}{\partial x}\left(\frac{1}{1+kx}\right) = -\frac{N^2 L_o k I^2}{2(1+kx)^2} \tag{15.10}$$

The minus sign indicates that the magnetic force tends to close the airgap x. In terms of the flux linkage λ, the force becomes:

$$F = -\frac{k\lambda^2}{2L_o N^2} \tag{15.11}$$

Defining a new variable, the maximum inductance:

$$L_{\max} = N^2 L_o \tag{15.12}$$

results in the following VHDL–AMS model equations:

$$\lambda = \frac{L_{\max} I}{1+kx}, \quad F_k = \frac{k}{2L_{\max}}, \quad F = -\lambda^2 F_k, \quad V = \frac{d\lambda}{dt} \tag{15.13}$$

The VHDL–AMS model includes two external electrical pins (nodes) and two mechanical pins. Given a current I and armature position x, the model equations compute λ and F. The value of F is passed to the mechanical pins as a variable. The voltage, the time derivative of λ, appears across the electrical pins.

Similar methods can be used to derive VHDL–AMS models for other magnetic components. First, the equations for stored energy, in terms of "across" and "through" variables, must be obtained. Then the forces, voltages, and losses in lossy cases, can be computed.

The VHDL–AMS solenoid model accepts a current value from electrical pins *p* and *m*, and a position value from mechanical pins *pos1* and *pos2*. The model entity parameters are listed in Table 15.1, and the VHDL–AMS entity description is in Table 15.2. The VHDL–AMS architecture code is listed in Table 15.3.

TABLE 15.1 VHDL–AMS Solenoid Model Entity Parameters

Interface	Name	Type	Default Value	Description
GENERIC	10	Inductance	1.25E–7	Maximum *L* for 1 turn
”	K	Real	197.735	*L* coefficient
”	N	Real	1.0	Number of coil turns
TERMINAL	*p, m*	Electrical	—	Electrical pins
”	*pos1*	Translational	—	Mechanical pin
”	*pos2*	Translational	—	Mechanical pin

TABLE 15.2 VHDL–AMS Solenoid Entity Description for Table 15.1

```
LIBRARY IEEE;
USE IEEE.ELECTRICAL_SYSTEMS.ALL;
USE IEEE.MECHANICAL_SYSTEMS.ALL;
ENTITY solenoid IS
  GENERIC (
    L0 : INDUCTANCE := 1.25e-7;
    K : REAL :=197.735;
    N : REAL :=1.0;
  PORT (
    TERMINAL p,m : ELECTRICAL;
    TERMINAL pos1, pos2 : TRANSLATIONAL);
    QUANTITY force_out : OUT REAL := 0.0);
END ENTITY solenoid;
```

TABLE 15.3 VHDL–AMS Solenoid Model Architecture Description

```
ARCHITECTURE behav OF solenoid IS
  CONSTANT Lmax : INDUCTANCE :=L0 * N * N;
  CONSTANT Fk : FORCE :=K / (2.0 * Lmax;
  QUANTITY v ACROSS i THROUGH p TO m;
  QUANTITY position ACROSS force THROUGH pos1 TO pos2;
  QUANTITY L : INDUCTANCE;
  QUANTITY flux : FLUX;
BEGIN
  IF (position > 0.0) USE
    L == Lmax / (1.0 + K * position);
  ELSE
    L == Lmax;
  END USE;
  flux == L * i;
  v == flux'DOT;
  force == flux * flux * Fk;
  force_out == -force;
END ARCHITECTURE behav;
```

Example 15.3 Simplorer VHDL–AMS Voltage Step Response of Solenoid The VHDL–AMS solenoid model described above is to be used to find the response to a step application of a 12-V automobile battery for 1 s. As shown in Figure E15.3.1, the total moving mass is 0.545 kg, and the force of gravity is included over the 0.0127-m stroke.

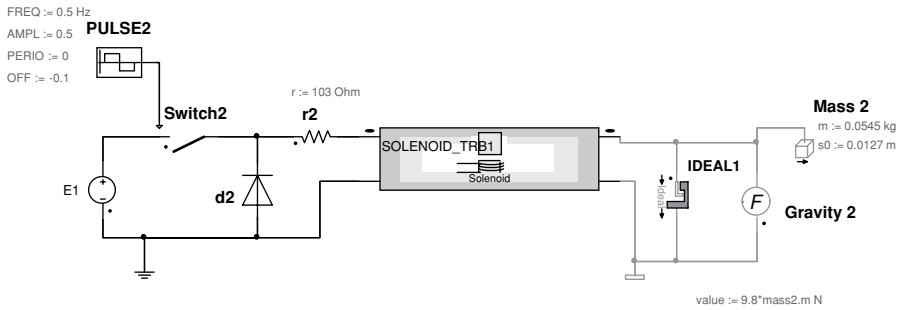

FIGURE E15.3.1 VHDL–AMS solenoid model in Simplorer with DC voltage switch.

The solenoid has 12,500 turns, a coil resistance of 103 Ω, and a diode connected as shown in Figure E15.3.1 to eliminate arcing at its switch upon turnoff. The solenoid constant k is not really a constant, and can be calculated in several ways. It can be found using the reluctance method of Chapter 3, the finite-element method of Chapter 4, and/or from measurements if the solenoid is available. In this example, finite-element solutions at two values of x are used. For $I = 0.084$ A and $x = 0$, $L = 1.251$E–7 H and $F = -27$ N. At the same current and $x = 0.0127$ m, $L = 3.56$E–8 H and $F = -0.84$ N. Find the current and force versus time from 0 to 2 s.

Solution The first approach to find k is to choose it to match L at both values of x. This should model the electrical side accurately at all times. Substituting the two L values in (15.5) gives $k = 197.735$.

Another approach is to match both L and F at time zero. Using (15.12) and (15.13) gives $L_{\max} = 19.547$ and then $\lambda = 1.642$. Substituting λ in (15.13) gives $F_k = 10$ and then $k = 391.52$.

The above two values of k are quite different. It is not possible to match both L and F over the whole solenoid operating range because of its nonlinear B–H steel, flux fringing, etc. The VHDL–AMS solenoid model thus is not as accurate as the preceding models using tables from finite-element analyses at far more than two positions. Thus the Simplorer SML modeling method of Section 15.1.6 can be more accurate than a Simplorer lumped parameter VHDL–AMS model.

To choose k, one might pick a compromise value of perhaps 300. If the mechanical behavior were more important, the 391.52 value might be chosen. Here the electrical behavior must be accurately modeled, so the value 197.735 is chosen.

The resulting current waveform computed by the VHDL–AMS capability of Simplorer is shown in Figure E15.3.2, along with the computed position versus time. The computed force versus time is shown in Figure E15.3.3. Note that the force takes time to build up after the voltage is applied at time zero, and takes time to decay after the voltage is switched off at time equal to 1 s.

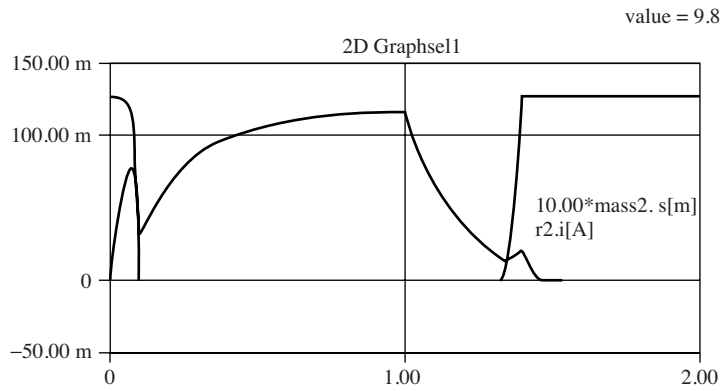

FIGURE E15.3.2 Current (slowly rising) and position versus time computed by VHDL–AMS model.

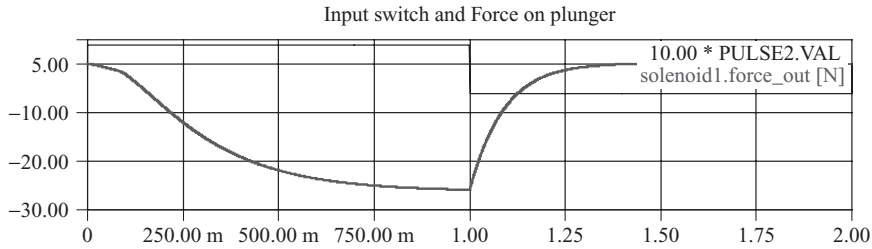

FIGURE E15.3.3 Force versus time computed by VHDL–AMS model.

15.3 MATLAB/SIMULINK MODELS

15.3.1 Software

MATLAB stands for matrix laboratory and was developed by Mathworks, Inc. A related software simulation package called Simulink is also popular.

MATLAB performs engineering calculations with and without matrices [6]. It is especially well suited for analyzing linear systems [7]. It offers a number of *toolboxes*, which are extensions for certain application areas. Its Control System Toolbox is commonly used by control systems engineers, and includes models in the Laplace transform s domain [8]. Alternative software exists such as Scilab, which is free.

Simulink provides an efficient graphical way for MATLAB users to model and simulate control systems in block diagram form. It includes many linear blocks and also some simple nonlinear blocks.

15.3.2 MATLAB Model of Voice Coil Actuator

The voice coil actuator of Chapter 7 has a force linearly proportional to current and thus is easily modeled using MATLAB as follows [9]. The model includes mechanical parameters such as M_S, B_S, and K_S of (15.3), which may be properties of a loudspeaker voice coil actuator.

Example 15.4 Step Response Times and Overshoot of Linear Voice Coil A voice coil actuator has the proportionality constant between voice coil current and magnetic force K_a, and thus:

$$F(t) = K_a I(t) \tag{E15.4.1}$$

The actuator is shown schematically in Figure E15.4.1, and has $K_a = 0.8$ N/A. The inductance of the coil is $L = 0.02$ H and its resistance shown externally is $R = 0.5\ \Omega$. Note that in this example $x(t)$ is the displacement and $u(t)$ is the velocity. The mass $M = 0.08$ kg, the damping friction is $B = 0.32$ N s/m, and the elasticity spring constant is $K = 1.6$ N/m.

To determine performance of the voice coil system using the approach commonly used by control systems engineers, the following tasks are to be performed:

(a) Write the equation for the electric circuit. Draw the force–voltage electric circuit analogy for the mechanical system and write the equation describing the mechanical system. Draw the s-domain (Laplace transform) block diagram for the electromagnetic actuator with $V(s)$ as the reference input and the displacement $X(s)$as the output. Mark all the s-domain variables $V(s)$, $I(s)$, $F(s)$, velocity $U(s)$, and position $X(s)$ on the block diagram and determine the transfer function $X(s)/V(s)$.

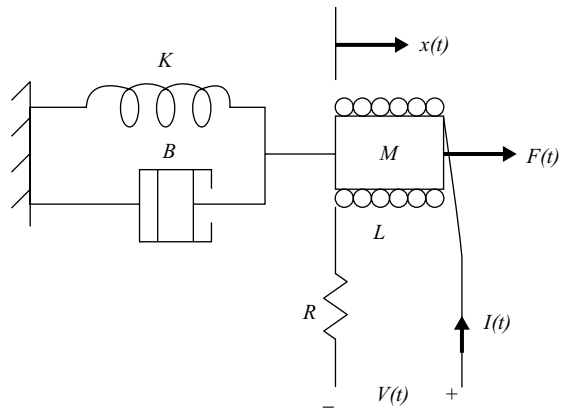

FIGURE E15.4.1 Voice coil actuator schematic diagram.

(b) Use the MATLAB *roots* function to find the roots of the system transfer function and determine the time constants. If one time constant is small relative to the other time constants, suggest a reduced-order model. Obtain the step response for the actual model and the reduced-order model on the same graph. After you have defined the numerators and denominators for both systems, you can use sys3rd = tf(num1, den1), and sys2nd = tf(num2, den2) to define the transfer function models. Then you can use:

```
ltiview('step', sys3rd, 'b', sys2nd, 'r')
```

to obtain the step response for both systems on the same linear time invariant (LTI) viewer. Right click on the plot area and determine the time domain characteristics, rise time t_r, peak time t_p, percent overshoot $P.O.$, and settling time t_s.

(c) The step response peak time and the percent overshoot of a second-order system is given by:

$$t_p = \frac{\pi}{\omega\sqrt{1-\zeta^2}} \quad \text{and} \quad P.O. = e^{\frac{-\zeta\pi}{\sqrt{1-\zeta^2}}} \times 100 \qquad \text{(E15.4.2)}$$

where ζ is the (dimensionless) damping ratio [8]. Using the above relations, compute t_p, $P.O.$, and the settling time $t_s = 4\tau$ for the reduced-order model and compare it to the value for the actual response found in (b).

Solution

(a) The time domain and the *s*-domain equivalent circuits for the electric circuit of the actuator and the force–voltage electric circuit analogy for the mechanical system is shown in Figure E15.4.2. Note that the motional voltage is assumed negligible.

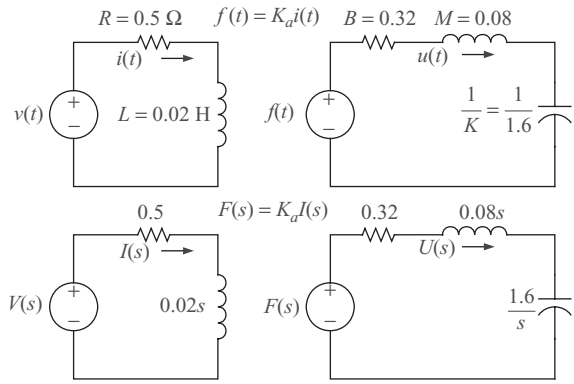

FIGURE E15.4.2 Time domain and *s*-domain equivalent circuits for voice coil actuator.

FIGURE E15.4.3 Block diagram of voice coil actuator.

From the s-domain equivalent circuit we have:

$$I(s) = \frac{1}{0.02\,s + 0.5}V(s) \quad \text{and} \quad U(s) = \frac{1}{0.08\,s + 0.32 + \dfrac{1.6}{s}}F(s) \tag{E15.4.3}$$

Also the given transducer equation:

$$F(s) = 0.8I(s) \tag{E15.4.4}$$

And the displacement in terms of velocity is:

$$X(s) = \frac{1}{s}U(s) \tag{E15.4.5}$$

The block diagram representing the above four equations is shown in Figure E15.4.3.

Thus the transfer function relating the s-domain displacement to the s-domain voltage is:

$$G(s) = \frac{X(s)}{V(s)} = \frac{0.8}{(0.02s + 0.5)\left(0.08s + 0.32 + \dfrac{1.6}{s}\right)s} \tag{E15.4.6}$$

or

$$G(s) = \frac{50}{(s + 25)(s^2 + 4s + 20)} = \frac{500}{s^3 + 29s^2 + 120s + 500} \tag{E15.4.7}$$

(b) The roots of the characteristic equation are:

$$\begin{aligned} r &= \text{roots}([1 \quad 29 \quad 120 \quad 500]) \\ r &= -25.0000 \\ &\quad -2.0000 + 4.0000i \\ &\quad -2.0000 - 4.0000i \end{aligned} \tag{E15.4.8}$$

The time constants are:

$$\tau_1 = \frac{1}{25} = 0.04 \quad \text{and} \quad \tau_2 = \frac{1}{2} = 0.5 \tag{E15.4.9}$$

$$G(s) = \frac{500}{25(0.04s+1)(s^2+4s+20)} = \frac{20}{(0.04s+1)(s^2+4s+20)} \tag{E15.4.10}$$

Note that $\tau_1 \ll \tau_2$. Neglecting the smaller time constant, the approximate second-order model becomes:

$$G(s) = \frac{20}{s^2+4s+20} \tag{E15.4.11}$$

To obtain the step response of the third-order and second-order systems, we use the following MATLAB commands.

```
num1 = 500; % third-order system num
den1 = [1 29 120 500]; % third-order system den
num2 = 20; % reduced-order system num
den2 = [1 4 20]; % reduced-order system den
sys3rd = tf(num1, den1) % third-order system
sys2nd = tf(num2, den2) % reduced-order system
ltiview('step', sys3rd, 'b', sys2nd, 'r')
```

The results are plotted in Figure E15.4.4.

(c) The second-order system characteristic equation is:

$$s^2 + 4s + 20 = 0 \tag{E15.4.12}$$

$$\omega_n^2 = 20 \Rightarrow \omega_n = 4.472 \tag{E15.4.13}$$

$$2\zeta\omega_n = 4 \Rightarrow \zeta = \frac{4}{2(4.472)} = 0.4472 \tag{E15.4.14}$$

$$t_p = \frac{\pi}{4.472\sqrt{1-0.4472^2}} = 0.785 \tag{E15.4.15}$$

$$P.O. = e^{\frac{-0.4472\pi}{\sqrt{1-0.4472^2}}} = 20.7 \tag{E15.4.16}$$

$$\tau = 1/(\zeta\omega_n) = 0.5 \text{ s} \tag{E15.4.17}$$

$$t_s = 4\tau = 2.0 \text{ s} \tag{E15.4.18}$$

The results are summarized in Table E15.4.1, which shows that the reduced-order model is a good approximation. The frequency response of the two systems can also be compared to again confirm the validity of the approximation.

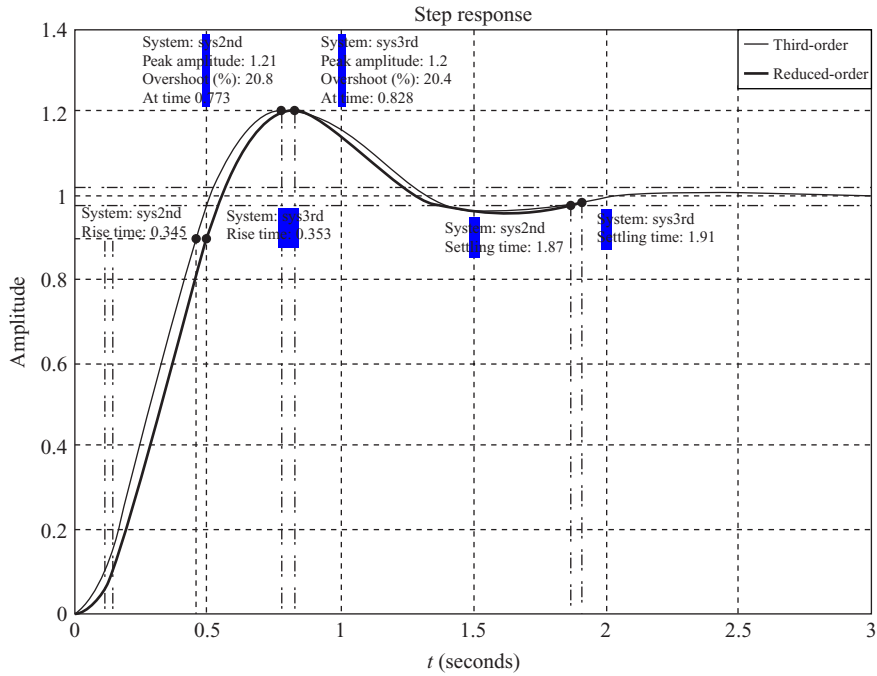

FIGURE E15.4.4 MATLAB plots of time domain response of voice coil actuator.

TABLE E15.4.1 Comparison of Responses of Systems Models of Actuator

Time Domain Specification	Third-order System Simulation Results	Reduced-order Simulation Results	Reduced Order Using Equation 15.4.2
Percent Overshoot	20.4%	20.8%	20.7%
t_p (s)	0.828	0.773	0.785
t_s (s)	1.91	1.87	2.0

Example 15.5 Frequency Response of Linear Voice Coil Actuator The frequency response of the voice coil actuator of Example 15.4 is to be found using MATLAB. Its Bode function is to be used to plot the response versus frequency for both the second-order and third-order models.

Solution The *m*-file commands are as follows.

```
L = 0.02; R = 0.5; K = 1.6; Kf = 0.8;
M = 0.08; B = 0.25;
num1 = Kf/(L*M); % third-order system numerator
den1 = [1 (B/M)+(R/L) (K/M)+(B/M)*(R/L) (K/M)*(R/L)];
                          % third-order system den
```

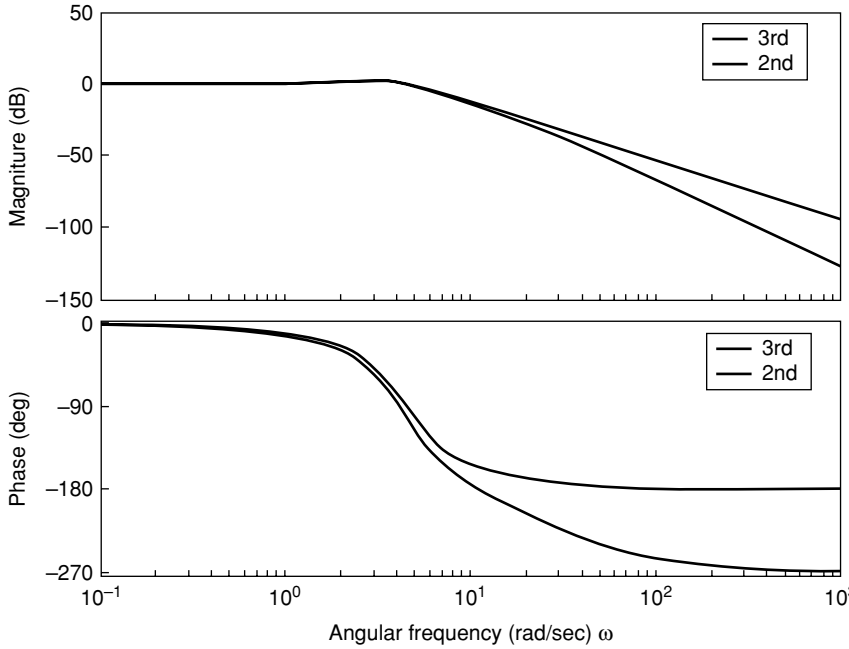

FIGURE E15.5.1 MATLAB bode plots of frequency domain response of voice coil actuator. At high frequencies the third-order model gives lower curves than the second-order model.

```
num2=num1/(R/L);          % reduced-order system numerator
den2 = [1 B/M K/M];       % reduced-order system denominator
sys3rd = tf(num1, den1)   % third-order system
sys2nd = tf(num2, den2)   % reduced-order system
disp('Example 15.4')
bode(sys3rd, 'b', sys2nd, 'r')
```

which obtain the Bode magnitude and phase plots shown above in Figure E15.5.1. Note that they agree closely at low frequencies but not at high frequencies. Note also that the peak magnitude occurs slightly above $\omega = 4$ rad/s. This is in reasonable agreement with the resonance formula $(K/M)^{1/2}$ of (14.21) that obtains $\omega = 4.47$ rad/s.

15.4 INCLUDING EDDY CURRENT DIFFUSION USING A RESISTOR

As discussed in Chapters 8 and 9, actuators and sensors made of solid steel can have significant eddy currents and associated diffusion time delays. One example is the Bessho DC axisymmetric plunger actuator, which is made of solid steel. Also, Example 9.2 has shown that planar devices also exhibit transient eddy currents. To

include transient eddy current diffusion effects in systems models, one method is to solve the eddy current finite-element model at each time step along with the systems solution, called *cosimulation* [10].

A simpler way to include eddy current effects in systems models is to add a resistor as described below. The resistor will first be derived for planar problems and then for axisymmetric problems.

15.4.1 Resistor for Planar Devices

The equivalent resistor for eddy current diffusion in a planar slab has been derived for linear *B–H* material of conductivity σ and a one-turn coil as [5]:

$$R_{EL1} = \pi^2 h_z/(\sigma\, h_y\, w) \tag{15.14}$$

where the material depth into the plane is h_z, its width in direction of diffusion is w, and its height in the remaining direction is h_y.

For a coil of N turns, the equation for linear eddy resistance in one slab is:

$$R_{EL} = (\pi N)^2 h_z/(\sigma\, h_y\, w) \tag{15.15}$$

Chapter 9 has shown that nonlinear *B–H* curves cause the diffusion time to change. To include nonlinear *B–H* effects, the eddy resistor is multiplied by the ratio of time constants:

$$R_E = (\tau_{mL}/\tau_{mN})(\pi N)^2\, h_z/(\sigma\, h_y\, w) \tag{15.16}$$

where τ_{mL} is the diffusion time of Chapter 9 for linear *B–H* and τ_{mN} is the diffusion time of Chapter 9 for nonlinear *B–H*.

Example 15.6 R_E for Inductor of Example 9.2 The eddy current resistor is to be found for the inductor of Example 9.2, shown in Figure E9.2.1, at a current of 0.5 A.

Solution The width $w = 0.02$ m, and the diffusion time ratio is $(\tau_{ml}/\tau_{mn}) = (54.6/18.9)$. Also, the total number of turns $N = (26.4)(2)(0.05/0.002) = 1320$. Also, the height $h_y = 0.05$ m and the depth $h_z = 0.1$ m. In addition, since the inductor has two legs (slabs), its power loss is doubled, and thus the eddy resistor of (15.14) must be divided by two, giving $R_E = 1462\ \Omega$.

Example 15.7 Simplorer Model of Inductor of Example 9.2 with Input Step Current and R_E The inductor of Example 9.2, shown in Figure E9.2.1, is to be modeled in Simplorer with an eddy current resistor added to account for linear magnetic diffusion. Its transient performance is to be computed when a step current of 0.5 A is input.

Solution From Example 15.6, the eddy current resistor is 1462 Ω. The magnetostatic flux linkage versus inductance is found by multiple Maxwell finite-element solutions of the model of Example 9.2 over a wide range of currents. The resulting Simplorer model is shown in Figure E15.7.1.

The input step current and computed output flux versus time are shown in Figure E15.7.2. Note that the flux is delayed somewhat less than the nonlinear diffusion time of 18.9 ms of Example 9.2. Since the diffusion time is the time for the center flux to rise, and most of the flux is outside the center of the leg, the Simplorer results are reasonable.

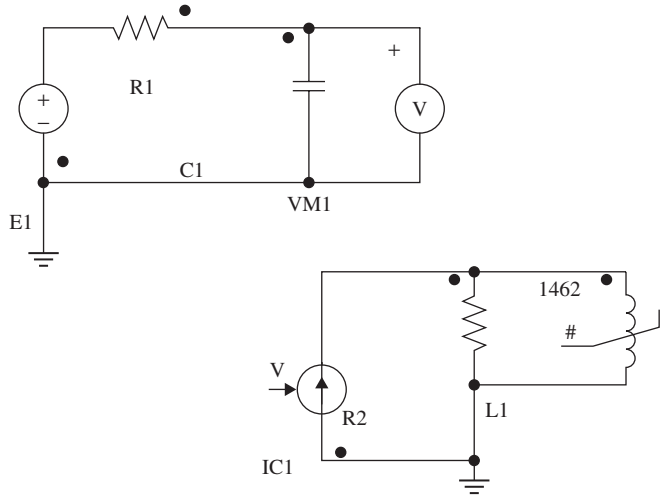

FIGURE E15.7.1 Simplorer model of inductor made of rectangular solid steel.

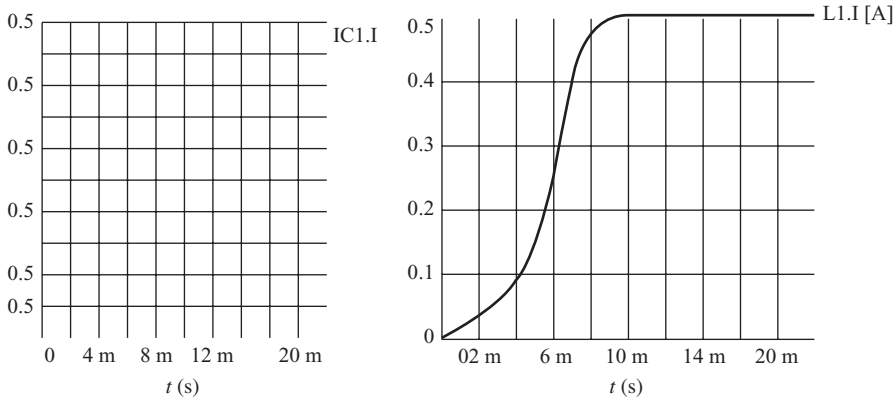

FIGURE E15.7.2 Current and flux obtained by Simplorer for Figure E15.7.1.

15.4.2 Resistor for Axisymmetric Devices

To derive the equivalent resistor for axisymmetric devices, begin with the constant permeability case. The classical formula for the resistance seen by current flowing peripherally on an arc around an axis is [3]:

$$R_{EL1} = \frac{4\pi}{2\sigma h \ln(b/a)} \tag{15.17}$$

where h is the axial length, b is outer radius, and a is inner radius. For a cylindrical armature and/or stator bore, the effective inner radius a varies with time according to the magnetic diffusion concept of Chapter 9, that is:

$$a = be^{-t/\tau_m} \tag{15.18}$$

Substituting (15.18) into (15.17) and referring resistance to the N turn stator winding gives the linear time-varying eddy current resistor [3]:

$$R_{EL} = 4\pi \frac{(N/k)^2}{2\sigma ht} \tag{15.19}$$

where the coupling coefficient k is not unity because the peripheral arc acts as a shorted turn and does not link all of the magnetic flux lines. Since both the flux and the eddy current decay together below the steel surface, k equals $\frac{1}{2}$. Also, time-varying resistors are not available in most versions of SPICE and other electric circuit software. Often the ratio (τ_m/t) is approximately unity at closing time, and thus (15.19) becomes approximately:

$$R_{EL} = 8\pi N^2/(\sigma h) \tag{15.20}$$

Besides adding this parallel resistor, it is also advisable to add a leakage inductor to prevent unrealistic current jumps. For the Bessho actuator, the SPICE model of Figure 15.1 has the added resistor R_{EL} and leakage inductor L_1 shown in Figure 15.6.

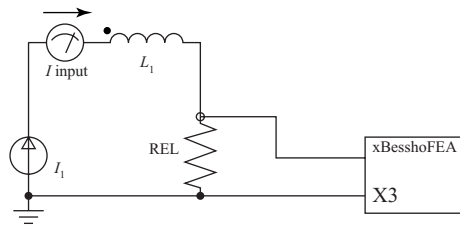

FIGURE 15.6 Adding leakage inductor L_1 and parallel resistor to SPICE model to account for eddy current diffusion.

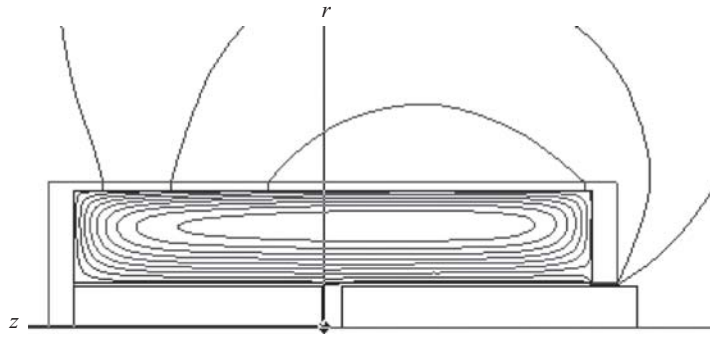

FIGURE 15.7 Computer display of flux line plot for Bessho actuator with flux excluded from steel, used to obtain value of leakage inductance L_1.

For the Bessho axial height of 0.27 m, $N = 3300$ and $\sigma = 1.7\text{E}6$ S/m, $R_{EL} = 596\ \Omega$. The leakage inductor L_1 is for flux that does not link the induced eddy currents. Thus L_1 is found by magnetostatic finite-element analysis of the actuator with its steel permeability set to the small value 0.1% of air. The resulting flux plot is shown in Figure 15.7 and the corresponding inductance L_1 is 65 mH.

To include nonlinear *B–H* effects, as shown earlier the resistance must be multiplied by the ratio of nonlinear to linear diffusion times. Thus the nonlinear eddy resistor is [11]:

$$R_{EN} = \left(\frac{\tau_{mL}}{\tau_{mN}}\right) \frac{8\pi N^2}{\sigma h} \tag{15.21}$$

where the nonlinear diffusion time τ_{mN} varies with applied field intensity H_o as described in Chapter 9. One must keep in mind, however, that the diffusion time calculations of Chapter 9 were for 1D problems, whereas airgaps and other 2D geometric features of real magnetic devices will cause changes in diffusion. Thus (15.21) is approximate, even when actuators are closed with "zero" airgap. No gap is exactly zero, but instead equals approximately 36 μm for polished steel surfaces [12].

For the Bessho actuator, Example 9.3 has found that $H_o = 6600$ A/m for the nominal current of 0.5 A. Using the actual Bessho steel *B–H* curves (not the step *B–H* curve of Example 9.3), the nonlinear diffusion time τ_{mN} computed by Maxwell finite-element analysis is 42 ms. Then the corresponding eddy resistor using (15.21) with $(\tau_{mL}/\tau_{mN}) = (93\ \text{ms}/42\ \text{ms})$ is $R_{EN} = 1320\ \Omega$ [11]. The resulting Simplorer output position for the same input current as Figure 15.5 is shown in Figure 15.8. The closing time is now 101 ms, increased by 4% from Figure 15.5, as expected from Table 14.1. Hence in this case the eddy currents cause only a 4% increase in operation time, but larger increases occur in other cases, as will be seen later in this chapter.

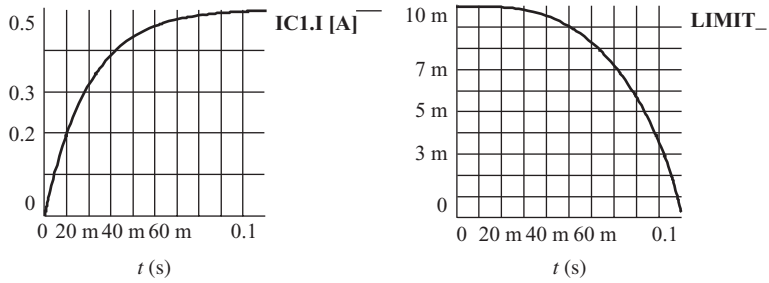

FIGURE 15.8 Computed Simplorer input and output for Bessho actuator including nonlinear 1320-Ω eddy resistor and 6-kg moving mass. The input on the left is the current (in amperes) waveform, and the output on the right is the airgap (in meters) as a function of time (in seconds).

15.5 MAGNETIC ACTUATOR SYSTEMS FOR 2D PLANAR MOTION

Besides the linear and rotary magnetic actuators discussed above and in previous chapters, magnetic actuators are increasingly being developed for 2D motion over a plane with optional motion in other degrees of freedom. Applications include pick-and-place machines for industry, inspection systems, and wafer scanners. In some cases magnetic bearings (levitators) are used [13] that are variations of the bearings discussed in Chapter 7. Alternative bearings include air bearings.

Planar actuators are typically designed to develop Lorentz force in either of the following two ways.

- A moving coil armature travels over a stator made with stationary permanent magnets. Like the voice coil actuator of Chapter 7, this type requires flexible connections to the moving coil.
- An armature made with permanent magnets travels over a stator made with current-carrying coils which do not require flexible connections. Thus the armature is said to be *contactless.*

Designs of planar magnetic actuators vary depending on stroke requirements. As mentioned in Chapter 7, commutation may be required for long strokes.

Figure 15.9 shows a recently developed planar actuator with a permanent magnet armature [14, 15]. It also has a manipulator energized by *contactless energy transfer* (CET) via inductive magnetic coupling. The control of the manipulator is by wireless link. The planar actuator uses commutation for long strokes in the *xy* plane, while the manipulator does the picking and placing of objects.

Designers of planar actuators face many challenges. The first challenge is the design of the magnetic suspension and propulsion that should be capable of levitating the heavy platform. Next, the planar actuator should have an unlimited long-stroke movement capability in the *xy* plane and short stroke in the other degree of freedom. In addition, the CET must be integrated in the system.

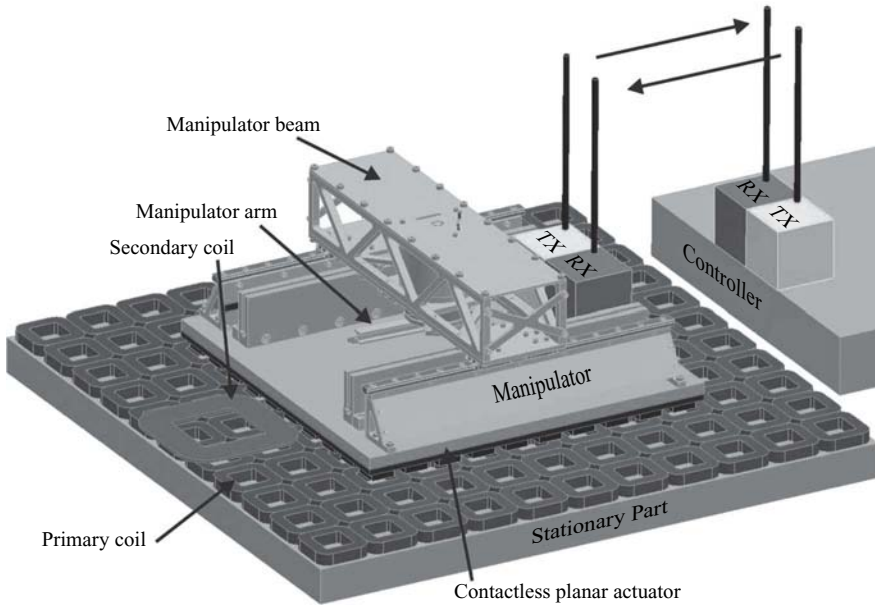

FIGURE 15.9 Contactless planar actuator with manipulator [14].

The heavy payload of the planar actuator requires large magnets and the use of a Halbach magnet array. Recall that Halbach magnets were discussed in Chapter 5. The coil topology is mainly determined by the design requirement to combine both magnetic actuation and CET by means of the same coil set. Rectangular coils are more efficient in generating forces than square or round coils. However, rectangular coils can only produce forces in two directions, so a pattern of rectangular coils in two orientations 90° apart is necessary to create forces in all three directions. Despite higher power loss to lift a certain mass, round coils are used in this system due to their suitability for CET. The final design of the planar actuator consists of a Halbach magnet array with 10×10 poles, with a pole pitch of 40 mm. The round coils are made of Litz wire to reduce power losses as mentioned in Chapter 12.

Sensors to control the planar actuator include both lasers and magnetic eddy current proximity sensors as discussed in Chapter 11. Preliminary results showed [14] that the planar actuator performed basic actuator functions, but had problems with its CET and long-stroke movements. More work is needed to perfect planar actuators.

15.6 OPTIMIZING MAGNETIC ACTUATOR SYSTEMS

Optimization of magnetic actuators as they operate electromechanical systems is achieved nowadays using finite-element software coupled to systems software. The

FIGURE 15.10 Two Delphi Multec® gasoline fuel injectors containing 3D magnetic actuators. Published with permission of Delphi Corporation. [16].

systems optimized here are a fuel injection system for automotive engines followed by a hydraulic valve actuated by a plunger solenoid.

15.6.1 3D Analysis of Fuel Injector System

Figure 15.10 shows two automotive fuel injectors manufactured by Delphi Corporation. They contain magnetic actuators similar to that shown in Figure 15.11. Note that one-half of the magnetic actuator is shown, which must be modeled in 3D to account for geometry details.

Some of the Maxwell software setup for the fuel injector system model is shown in Figure 15.12. Note that both electrical and mechanical design variables are described. The empirically obtained load force equation involves the injector parameters and is specified by inputting code (where $*$ symbolizes multiply and $**2$ symbolizes 2nd power) [16]:

$$F_{\text{load}} = (-(2 + \text{k} * \text{Position}) - \text{weight} - (\pi * \text{FuelP} * \text{sealdia} * *2/ \\ (4 * (1 + \text{PressRatio} * (\text{Position}/\text{maxstroke}) * *2)))) \qquad (15.22)$$

Also part of the Maxwell input is the schematic circuit shown in Figure 15.13. As in Example 15.3, a diode is used in the switching circuit.

The computed current, armature speed, and flux versus time are plotted in Figure 15.14. Note that the speed increases until the armature closes the gap at time approximately equal to 0.7 ms.

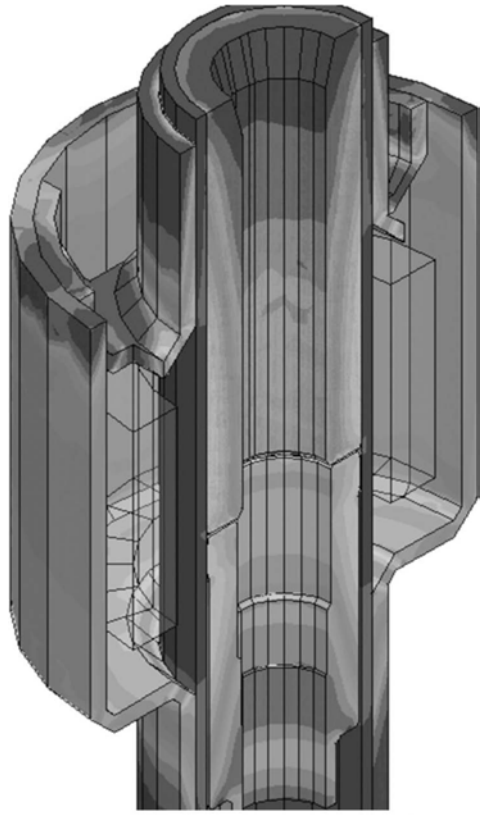

FIGURE 15.11 One-half of 3D magnetic actuator for fuel injector of Figure 15.10. Published with permission of Delphi Corporation and ANSYS, Inc. [16].

Next the moving mass was increased by 50% and the optimum design was sought by varying the wire gauge and number of turns while maintaining the coil resistance. This was accomplished using many parametric analyses on several computers simultaneously, a method called *distributed processing*. Alternative optimization methods include *genetic optimization*, which imitates the evolutionary process of biological natural selection [17].

Parametric results were obtained with and without conductivity in the solid steel armature and stator. Figure 15.15 graphs the current versus time plotted without conductivity, that is, with no eddy currents and zero diffusion time. Figure 15.16 graphs the current versus time computed with actual finite-steel conductivity. Note that the dip in the current waveform indicates closing time, which is made longer (as expected) by the diffusion time in the conducting steel. Note also the variation with wire size, which helps the designer choose the wire size and coil turns. The faster the closing time, the more accurate is the fuel injection, which reduces hydrocarbon emissions by the automotive gasoline engine.

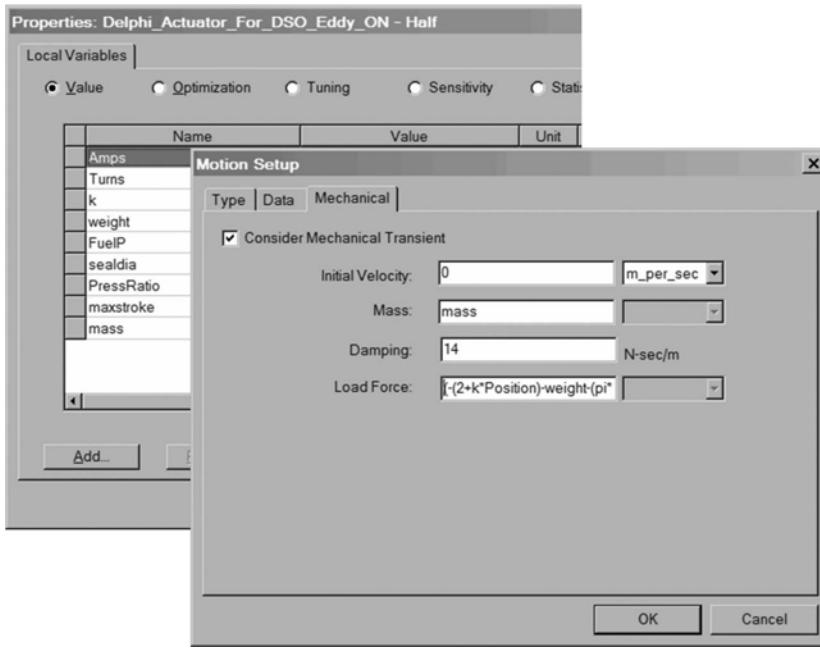

FIGURE 15.12 Input parameters for optimized design of fuel injector of Figure 15.11. Published with permission of Delphi Corporation and ANSYS, Inc. [16].

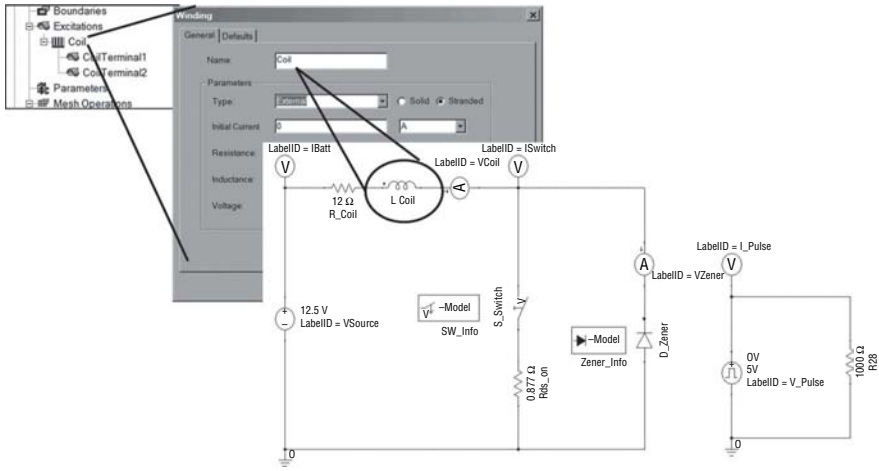

FIGURE 15.13 Schematic of circuit input for fuel injector of Figure 15.11. Published with permission of Delphi Corporation and ANSYS, Inc. [16].

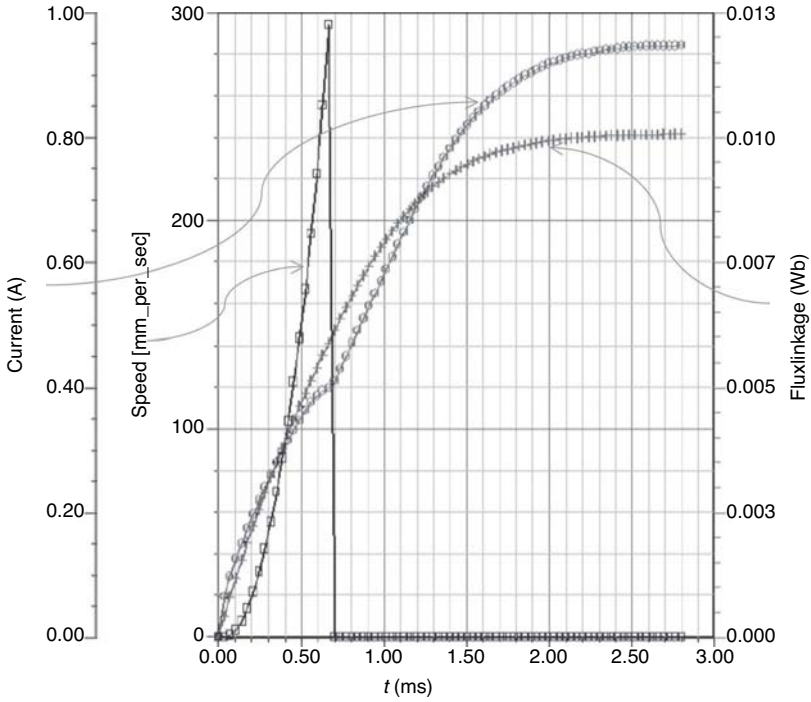

FIGURE 15.14 Computed results for current, speed, and flux for half model of fuel injector of Figure 15.11. Note that the armature closes in approximately 0.7 ms. Published with permission of Delphi Corporation and Ansys, Inc. [16].

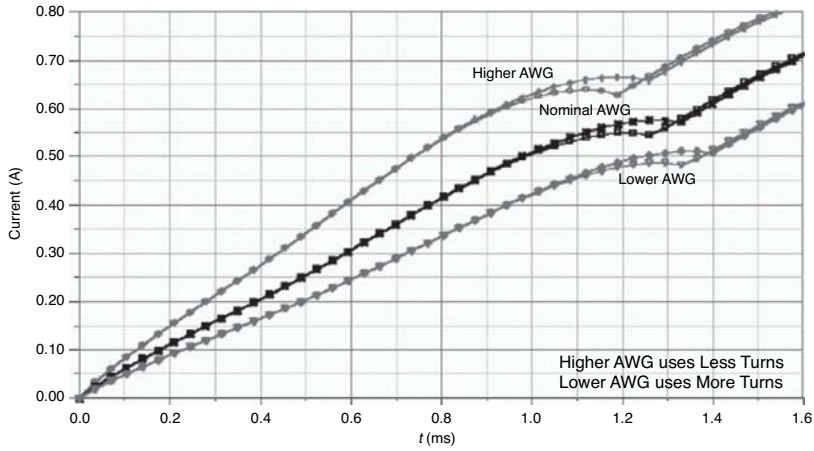

FIGURE 15.15 Computed current waveforms for zero conductivity in the magnetic actuator of Figure 15.11. The dips occur at closing time. Each curve pair has two slightly different curves for nominal mass and half nominal mass, the half mass closing slightly faster. The AWG wire gauge was varied to maintain the same coil resistance. Published with permission of Delphi Corporation and Ansys, Inc. [16].

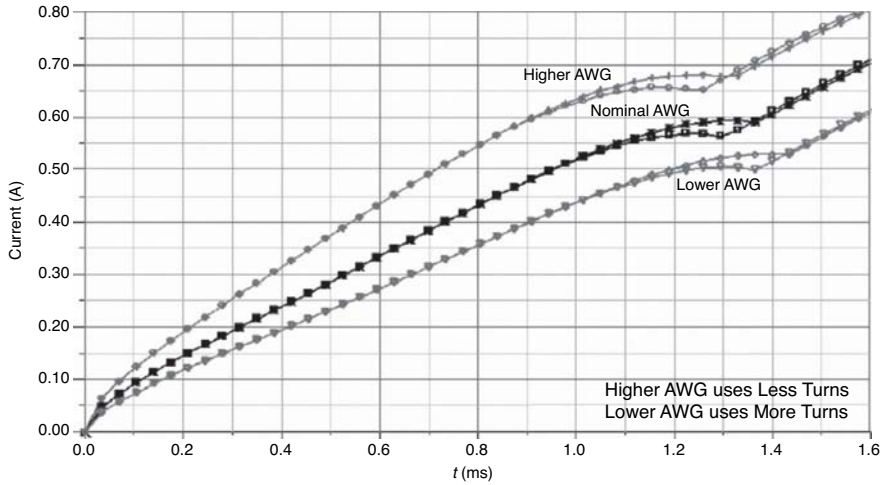

FIGURE 15.16 Computed current waveforms including diffusion time for actual conductivity in the magnetic actuator of Figure 15.10. The dips occur at closing time. Each curve pair has two slightly different curves for nominal mass and half nominal mass, the half mass closing slightly faster. The AWG wire gauge was varied to maintain the same coil resistance. Published with permission of Delphi Corporation and ANSYS, Inc. [16].

15.6.2 Analysis of 3D Solenoid for Valve Actuation

Engineers designing solenoid actuators for applications such as hydraulic valves need to optimize the entire system. The system design method used on a TRW Automotive application is outlined in Figure 15.17 [18]. The lower portion shows the schematic of a typical solenoid driving a typical hydraulic system (such as discussed in the next chapter). The design method begins with 2D axisymmetric magnetic finite-element analysis, but then includes 3D magnetic finite-element analysis as well as thermal analysis (discussed in Chapter 12) and finally uses optimization software to achieve the best system design. Optimum solenoid design meets force versus stroke requirements, fits in the space available, and operates within a specified closing time. The solenoid design must also meet thermal requirements and be integrated into the entire system function. Systems optimized include antilock brakes, traction control, electronic stability control, and adaptive cruise control.

The solenoid to be optimized is shown in Figure 15.18. An approximate initial model is the axisymmetric 2D model, but later the more accurate 3D model will be optimized. The coil design equations are incorporated as design variables in Maxwell, with the wire gauge input by the designer. Based on coil space, the software then easily calculates the number of turns and the coil resistance. For all of the various wire gauges, parametric finite-element analyses compute the performance over a range of coil currents and armature positions. The parametric ranges can also include armature and stator shapes, material changes, etc. Computed performance includes the static magnetic force versus current. Figure 15.19 shows that the computed force curve

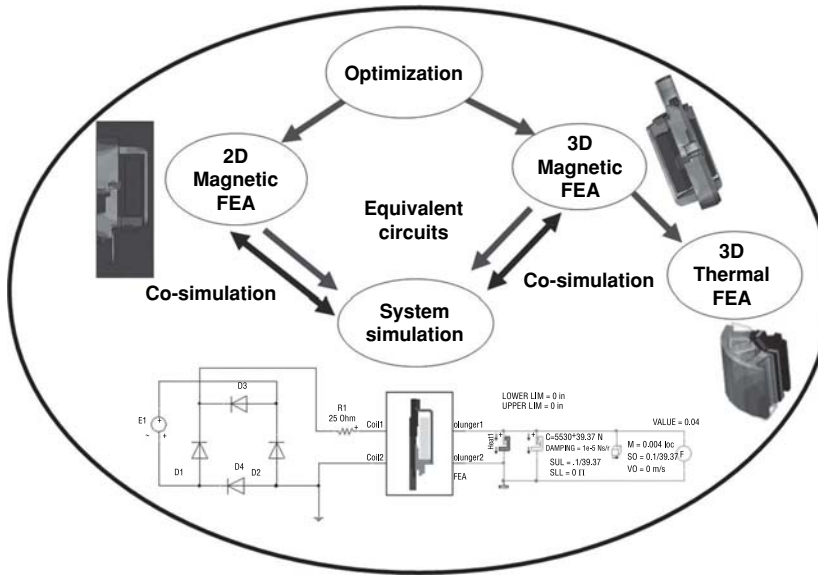

FIGURE 15.17 Design method for solenoid actuators driving hydraulic systems. Published with permission of TRW Automotive and ANSYS, Inc. [18].

compares very well with the measured force curve, which varies as shown due to friction.

Next the dynamic performance of the solenoid, including eddy currents and magnetic diffusion, is computed. Figure 15.20 shows the dynamic (or transient) drive circuit model of the actuator, which is driven by a voltage source and switches controlled by subcircuits. The computed waveforms of current and position are shown in Figure 15.21. Note that the voltage is initially switched to a high value to move the armature quickly, and then the current is reduced electronically between upper and lower limits to maintain closure, ending with switch-off and the armature moving back to its initial zero position.

After computing the above performance of the base solenoid electromechanical model, optimization of the solenoid system was carried out in the following steps. First, the shape of the actuator pole was varied to meet the mechanical spring curve. The spring curve is made by two springs as shown in Figure 15.22, which also shows typical magnetic pull curves for different pole shapes. The intersection of the magnetic curve and the spring curve is the operating position of the armature. The magnetic pull curves are of course affected by the magnetic circuit, including the details of the armature and stator shapes and the airgap. The dimensional variables in the airgap region are shown in Figure 15.23, all of which were input parametric variables in the Maxwell 3D finite-element analysis.

As the optimization software ran through the design variables of Figure 15.23, it was first programmed to minimize the *cost function* that meets the spring curve of Figure 15.22 at the critical maximum force points. The pole shape optimized design,

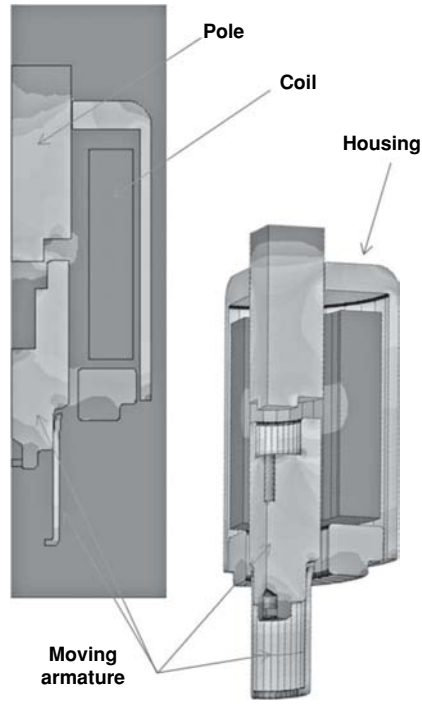

FIGURE 15.18 Typical solenoid to be optimized for use in a hydraulic system. A 2D axisymmetric model and a 3D model are shown. Published with permission of TRW Automotive and ANSYS, Inc. [18].

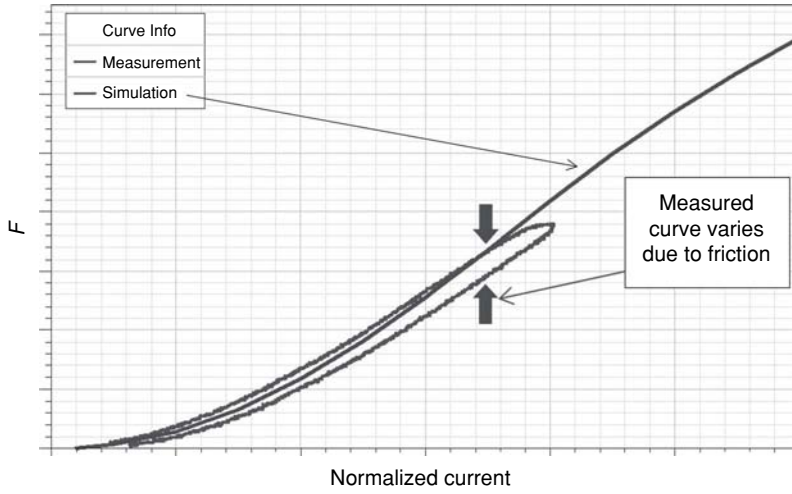

FIGURE 15.19 Computed and measured curves of static magnetic force versus coil current for solenoid of Figure 15.18. Published with permission of TRW Automotive and ANSYS, Inc. [18].

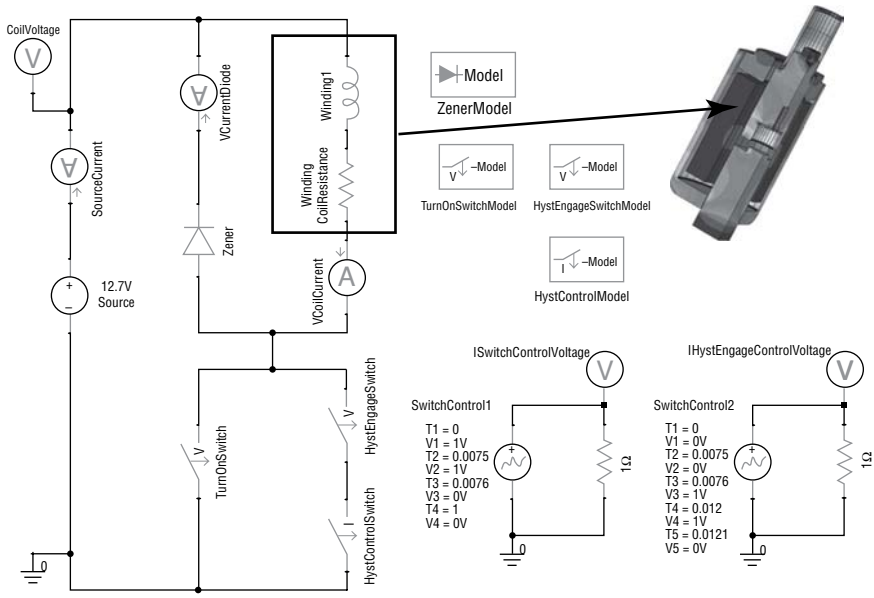

FIGURE 15.20 Circuit schematic of transient Maxwell model of solenoid of Figure 15.18. Published with permission of TRW Automotive and ANSYS, Inc. [18].

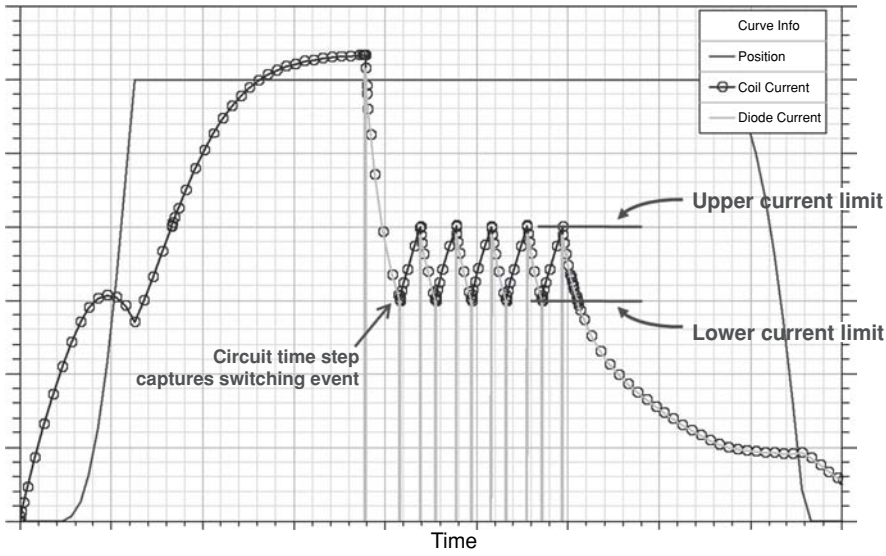

FIGURE 15.21 Computed coil current and position versus time for solenoid model of Figure 15.18. Published with permission of TRW Automotive and ANSYS, Inc. [18].

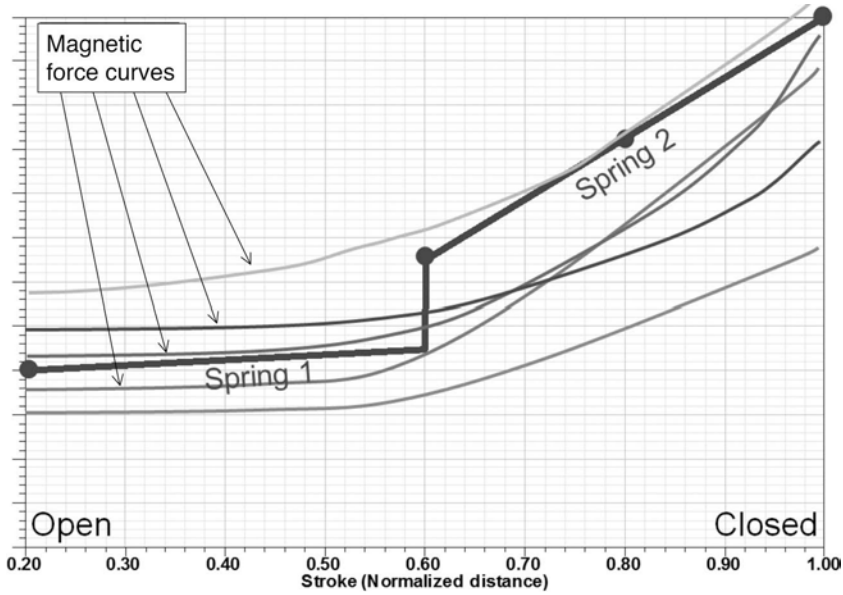

FIGURE 15.22 Mechanical spring forces and typical magnetic forces versus position for solenoid model of Figure 15.18. Published with permission of TRW Automotive and Ansys, Inc. [18].

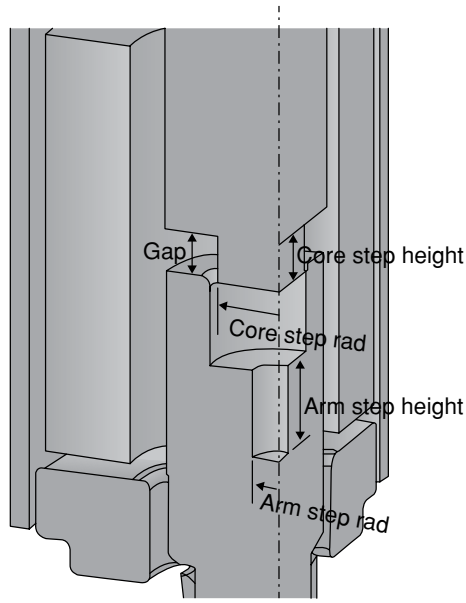

FIGURE 15.23 Dimensional variables for 3D model of solenoid of Figure 15.18. Published with permission of TRW Automotive and Ansys, Inc. [18].

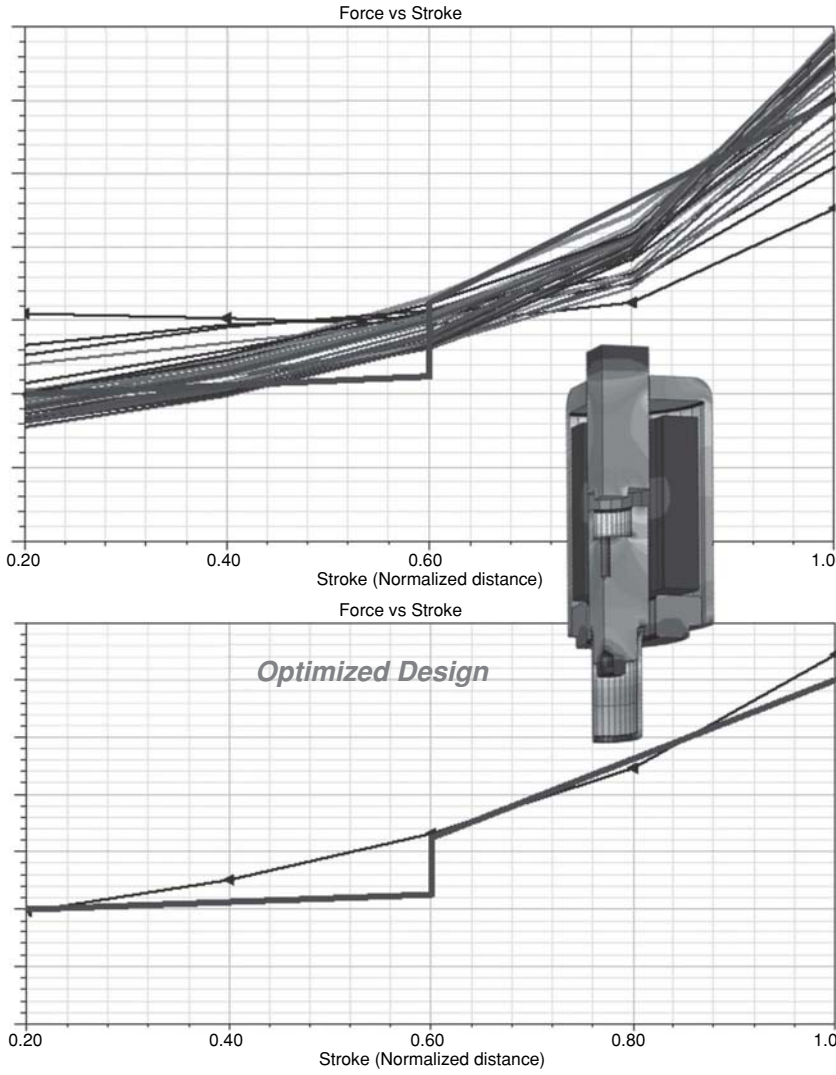

FIGURE 15.24 Graphs of force versus position for 3D model of solenoid of Figure 15.18. The upper graph has many curves for many design iterations. The lower graph shows the final magnetic pull curve and the mechanical spring curve. Published with permission of TRW Automotive and Ansys, Inc. [18].

achieved after about 50 design iterations, is shown in Figure 15.24 and meets the force curve.

The next optimization was for the cost function set to minimize the closing time of the solenoid in its electromechanical system. Again the 3D Maxwell transient model was used along with the related Optimetrics software, but the input variable this time was the number of coil turns. The families of position and current versus time curves

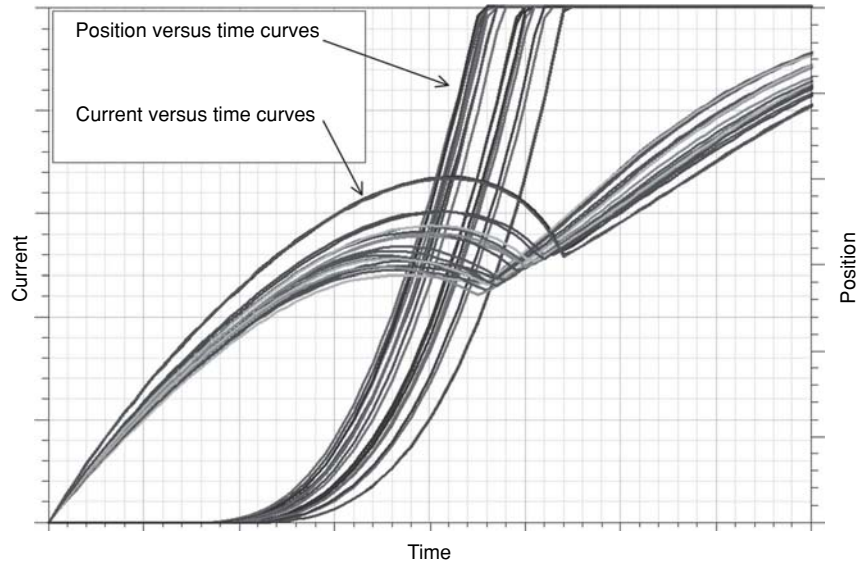

FIGURE 15.25 Curves of position and coil current versus time for various numbers of coil turns in solenoid of Figure 15.24. Published with permission of TRW Automotive and ANSYS, Inc. [18].

are shown in Figure 15.25. Note that the closing time can be greatly reduced by the proper choice of the number of coil turns.

Further optimization of this solenoid for operation of a hydraulic valve will be presented in the next chapter.

PROBLEMS

15.1 Redo Example 15.1 for the coil resistance increased (using smaller diameter wire) by 50%. Use the electric circuit software of your choice.

15.2 Redo Example 15.1 for the coil resistance increased (using smaller diameter wire) by 100%. Use the electric circuit software of your choice.

15.3 Redo Example 15.2 with $V_{\text{speed}} = 11t^2$.

15.4 Redo Example 15.2 with $V_{\text{speed}} = 9t^2$.

15.5 Redo VHDL–AMS Example 15.3 with the solenoid constant $k = 391.5$.

15.6 Redo VHDL–AMS Example 15.3 with the solenoid constant $k = 300$.

15.7 Redo MATLAB Example 15.4 with mass reduced to 0.06 kg.

15.8 Redo MATLAB Example 15.4 with damping reduced to 0.25 N s/m.

15.9 Redo MATLAB Example 15.5 with mass reduced to 0.06 kg.

REFERENCES

1. Kielkowski R. *Inside SPICE*. McGraw-Hill, Inc.; 1994.
2. McDermott TE, Zhou P, Gilmore J, Cendes ZJ. Electromechanical system simulation with models generated from finite element solutions. *IEEE Trans Magn* 1997;33:1682–1685.
3. Brauer JR, Chen QM. Alternative dynamic electromechanical models of magnetic actuators containing eddy currents. *IEEE Trans Magn* 2000;36:1333–1336.
4. *Simplorer V7 VHDL–AMS Tutorial*. Pittsburgh, PA: ANSYS, Inc.; 2004.
5. Woodson HH, Melcher JR. *Electromechanical Dynamics*. New York: John Wiley & Sons; 1968.
6. Hanselman D, Littlefield B. *Mastering MATLAB® 6*. Upper Saddle River, NJ: Prentice Hall; 2001.
7. Strum RD, Kirk DE. *Contemporary Linear Systems Using MATLAB®*. Pacific Grove, CA: Brooks/Cole; 2000.
8. Dorf RC, Bishop RH. *Modern Control Systems*, 9th ed. Upper Saddle River, NJ: Prentice Hall; 2001.
9. Saadat H. *Control Systems Laboratory Manual*. Milwaukee, WI: Milwaukee School of Engineering; 2003.
10. Zhou P, Lin D, Fu WN, Ionescu B, Cendes ZJ. A general co-simulation approach for coupled field-circuit problems. *IEEE Trans Magn* 2006;42:1051–1054.
11. Brauer JR, Mayergoyz ID. Finite element computation of nonlinear magnetic diffusion and its effects when coupled to electrical, mechanical, and hydraulic systems. *IEEE Trans Magn* 2004;40:537–540.
12. Roters HC. *Electromagnetic Devices*. New York: John Wiley & Sons; 1941.
13. Jansen JW, van Lierop CMM, Lomonova EA, Vandenput AJA. Magnetically levitated planar actuators with moving magnets. *IEEE Trans Indust Appl* 2008;44:1108–1115.
14. deBoeij J, Lomonova E, Duarte J. Contactless planar actuator with manipulator: a motion system without cables and physical contact between the mover and the fixed world. *IEEE Trans Indust Appl* 2009;45:1930–1938.
15. Lomonova E. Advanced actuation systems—state of the art: fundamental and applied research. *Proceedings of the International Conference on Electrical Machines and Systems*, October 10–13, 2010, pp 13–24.
16. Solveson M, Steward D, Mastro N. Design optimization of fast-acting actuators including eddy current effects and diffusion. Presentation at *ANSYS Inspiring Engineering Workshop*, Southfield, MI, October, 2007.
17. Pellikka M, Ahola V, Söderlund L, Uusitalo J-P. Genetic optimization of a fast solenoid actuator for a digital hydraulic valve. *Int J Fluid Power* 2011;12:49–56.
18. Solveson M, Christini M, Collins D. Actuator design: Meeting your customer's requirements for success. Presentation at *ANSYS First-pass System Success Workshop*, Southfield, MI, October, 2008.